Elliptic flow of thermal photons in heavy-ion collisions at energies available at the BNL Relativistic Heavy Ion Collider and at the CERN Large Hadron Collider

H. Holopainen,[*] S. S. Räsänen,[†] and K. J. Eskola[‡]

Department of Physics, P.O. Box 35, FIN-40014 University of Jyväskylä, Finland and

Helsinki Institute of Physics, P.O. Box 64, FIN-00014 University of Helsinki, Finland

We calculate the thermal photon transverse momentum spectra and elliptic flow in $\sqrt{s_{NN}} = 200$ GeV Au + Au collisions at the Relativistic Heavy Ion Collider (RHIC) and in $\sqrt{s_{NN}} = 2.76$ TeV Pb + Pb collisions at the Large Hadron Collider (LHC), using an ideal hydrodynamical framework which is constrained by the measured hadron spectra at RHIC and LHC. The sensitivity of the results to the QCD-matter equation of state and to the photon emission rates is studied, and the photon v_2 is discussed in light of the photonic p_T spectrum measured by the PHENIX Collaboration. In particular, we make a prediction for the thermal photon p_T spectra and elliptic flow for the current LHC Pb + Pb collisions.

PACS number(s): 12.38.Mh, 25.75.Cj, 25.75.Ld

I. INTRODUCTION

Experimental data at the Relativistic Heavy Ion Collider (RHIC) and now also at the Large Hadron Collider (LHC) have shown compelling evidence of strongly interacting QCD-medium production in ultrarelativistic heavy-ion collisions. The measured transverse energies, transverse momentum (p_T) spectra, and, in particular, the significant azimuthal anisotropy (elliptic flow) of final-state hadrons suggest together that partonic QCD matter, quark-gluon plasma (QGP), is formed in these collisions.

In the collision of two nuclei, the azimuthally anisotropic overlap region sets preferred directions for the transverse flow. In hydrodynamical models, pressure gradients turn the spatial anisotropy of the produced hot matter into a flow anisotropy, which is transmitted into the momentum distributions of measurable final-state hadrons at the decoupling of the system. However, the hadronic measurement reflects the flow (and temperature) conditions only in the freeze-out region where the hadronic interactions cease.

In comparison with partons, photons interact only very weakly with the QCD matter and thus a photon emitted from the medium most likely escapes from the system without interacting. This is seen also in the measurements where photons do not show a similar suppression as hadrons when we move from proton+proton ($p + p$) to nucleus+nucleus ($A + A$) collisions [1]. Since photons can escape from the medium without interacting, they carry information about the system at the time of their production.

Ultrarelativistic heavy-ion collisions are particularly interesting in regard to direct photon production, since relative to $p + p$ collisions there are different types of nuclear effects at work as well as a number of important further sources for photons. In $p + p$ (and also in $p + A$) collisions the direct photons are prompt photons originating from the primary hard

interactions of partons, and fragmentation photons emitted by the primarily produced high-p_T partons [2]. In heavy-ion collisions (and also in $p + A$ collisions), both the prompt and fragmentation photons at high p_T are subjected to nuclear effects in the parton distribution functions of the colliding nuclei (see, e.g., Refs. [3,4] for the quantification of these effects and their uncertainties). The fragmentation photon component, however, is expected to be suppressed due to the quenching of partonic jets in QCD matter in $A + A$ collisions. In addition to this, in $A + A$ collisions the jet (parton)-matter interactions, i.e., the jet-photon conversion [5,6] and collision-induced photon emission from high-energy partons, can produce photons which are important in the mid-p_T region [7–9]. Finally, the hot medium itself emits thermal photons, which are expected to be important in the few-GeV region and below, as discussed in the hydrodynamical studies of Refs. [7,8,10–13].

In heavy-ion collisions, it is very difficult to distinguish between the different direct photon sources. In addition, there is a huge decay-photon background to deal with. The elliptic flow of direct photons could, however, shed more light on the interplay of the various photon production sources, which differ from each other as follows: At high p_T (above $\sim$5 GeV at RHIC), where prompt photons dominate [7] and where the fragmentation photons are more suppressed in the out-of-plane direction (perpendicular to the impact parameter), the photonic v_2 should be positive but very small [9]. The jet-medium interactions in turn increase the photon production most strongly in the in-plane direction (parallel to the impact parameter), thus causing a negative v_2 contribution at mid p_T [9]. The thermal photon production is affected by the hydrodynamical transverse flow itself, so photons in the in-plane direction get a stronger boost. As shown earlier in Refs. [14–17], this results in a positive elliptic flow for the thermal photons. Because the net contribution from other sources to photon v_2 is expected to be very small or even negative [9], a large (hadron-like) photon v_2 measured in the few-p_T region and below should thus serve as a signature of thermal photon dominance. Since QCD matter is emitting photons throughout its entire evolution, measuring thermal

———————
[*]hannu.l.holopainen@jyu.fi
[†]sami.s.rasanen@jyu.fi
[‡]kari.eskola@phys.jyu.fi

photon p_T spectra and v_2 would thus give important further constraints for the dynamics and properties of QCD matter.

In this work we focus on computing the thermal photon p_T spectra and elliptic flow in $\sqrt{s_{NN}} = 200$ GeV Au + Au collisions at RHIC and in $\sqrt{s_{NN}} = 2.76$ TeV Pb + Pb collisions at the LHC, using an ideal hydrodynamical framework which is constrained by the measured hadron spectra at RHIC and LHC. We study the sensitivity of the results to the QCD-matter equation of state (EoS) and to the photon emission rates. We discuss the photon v_2 in light of the photonic p_T spectrum measured by the PHENIX Collaboration [18–20]. In particular, we make a prediction for the thermal photon p_T spectra and elliptic flow for the current LHC heavy-ion collisions. Previous predictions for the thermal photon p_T spectra in Pb + Pb collisions at the planned maximum center-of-mass energy of 5.5 TeV of the LHC can be found in Refs. [21,22].

II. THEORETICAL FRAMEWORK

A. Centrality classes

Centrality classes for $A + A$ collisions studied here are calculated using the optical Glauber model. For nuclear densities we use spherically symmetric Woods-Saxon profiles with the the thickness parameter $d = 0.54$ fm and radii $R_{Au} = 6.37$ fm and $R_{Pb} = 6.49$ fm. The total cross section for $A + A$ collisions is calculated from

$$\sigma_{tot}^{AA} = \int d^2\boldsymbol{b} \frac{d\sigma_{tot}}{d^2\boldsymbol{b}} = \int d^2\boldsymbol{b}(1 - e^{-T_{AA}(\boldsymbol{b})\sigma_{NN}^{in}}), \quad (1)$$

where T_{AA} is the standard nuclear overlap function and σ_{NN}^{in} is the inelastic nucleon-nucleon cross section. We take $\sigma_{NN}^{in} = 42(64)$ mb for $\sqrt{s_{NN}} = 200 (2760)$ GeV.

The centrality classes are defined with impact parameter ranges $[b_i, b_{i+1}]$ so that for the centrality class of c_i we have

$$c_i = \frac{1}{\sigma_{tot}^{AA}} \int_{b_i}^{b_{i+1}} d^2\boldsymbol{b}(1 - e^{-T_{AA}(\boldsymbol{b})\sigma_{NN}^{in}}). \quad (2)$$

The average impact parameter for each centrality class is calculated using the distribution $d\sigma/d^2\boldsymbol{b}$ as a weight. The average number of participants is calculated similarly. The obtained centrality classes, impact parameter ranges, average impact parameters, and number of participants are listed in Table I.

B. Initial states for hydrodynamical evolution

For RHIC we use the EKRT saturation model [23] to fix the initial entropy in most central collisions. As shown in Refs. [24,25] we can get a good description of the pion spectra and the elliptic flow with this pQCD + saturation + hydrodynamics approach. For Au + Au collisions at $\sqrt{s_{NN}} = 200$ GeV the model gives an initial time $\tau_0 = 0.17$ fm. For the $\sqrt{s_{NN}} = 2.76$ TeV Pb + Pb collisions at the LHC, we fix the initial entropy so that we reproduce the measured multiplicity [26]. The initial time $\tau_0 = 0.12$ fm is based on the EKRT-motivated fit performed in Ref. [27].

TABLE I. Various centrality classes for Au + Au collisions at $\sqrt{s_{NN}} = 200$ GeV and for Pb + Pb collisions at $\sqrt{s_{NN}} = 2.76$ TeV, obtained via the optical Glauber model.

	Centrality (%)	Range of b (fm)	$\langle b \rangle$ (fm)	N_{part}
RHIC	0–5	0.00–3.35	2.24	346
	5–10	3.35–4.74	4.08	289
	10–15	4.74–5.81	5.30	242
	15–20	5.81–6.71	6.27	202
	20–30	6.71–8.21	7.49	153
	30–40	8.21–9.49	8.87	102
	40–50	9.49–10.6	10.1	64.4
	50–60	10.6–11.6	11.1	37.5
	0–20	0.00–6.71	4.47	267
	20–40	6.71–9.49	8.18	128
LHC	0–5	0.00–3.53	2.35	375
	0–20	0.00–7.05	4.70	294
	20–40	7.05–9.98	8.60	141

To fix the initial transverse density profile in $\sqrt{s_{NN}} = 200$ GeV Au + Au collisions, we do the following: In Fig. 1 we show, from Ref. [28], the measured charged-particle multiplicity (divided by the number of participant pairs) as a function of the number of participants calculated from the optical Glauber model.[1] Choosing the initial transverse density according to the binary-collision-scaled energy or entropy density (eBC, sBC), or wounded-nucleon-scaled energy or entropy density (eWN, sWN) as introduced in Ref. [29], we compute the charged-particle multiplicity in the centrality classes obtained earlier. The initial entropy at $b = 0$ in these four cases is kept fixed. We see that the sWN profile fits the measured centrality dependence quite well. We therefore choose the sWN profile at RHIC and, for simplicity, use the same profile also for the LHC Pb + Pb collisions.

C. Hydrodynamics and freeze-out

To describe the space-time evolution of the produced QCD matter, we solve the ideal hydrodynamical equations

$$\partial_\mu T^{\mu\nu} = 0, \quad (3)$$

where $T^{\mu\nu} = (\epsilon + P)u^\mu u^\nu - Pg^{\mu\nu}$ is the energy-momentum tensor, u^μ is the fluid four-velocity, ϵ is the energy density, and P is the pressure. Because we are interested in particle and photon production at midrapidity, we may assume that net-baryon density is negligible. Because the particle spectra are approximately flat at midrapidity, we can simplify our hydrodynamical equations by assuming longitudinal boost invariance. We use the SHASTA algorithm [30,31] to solve this (2 + 1)-dimensional numerical problem.

To close the hydrodynamic equations we need an equation of state, $P = P(\epsilon)$. In this paper we study the sensitivity of thermal photon production to the EoS by focusing on two

_____

[1]Note that the number of participants quoted by the experiments here is usually from the Monte Carlo Glauber model.
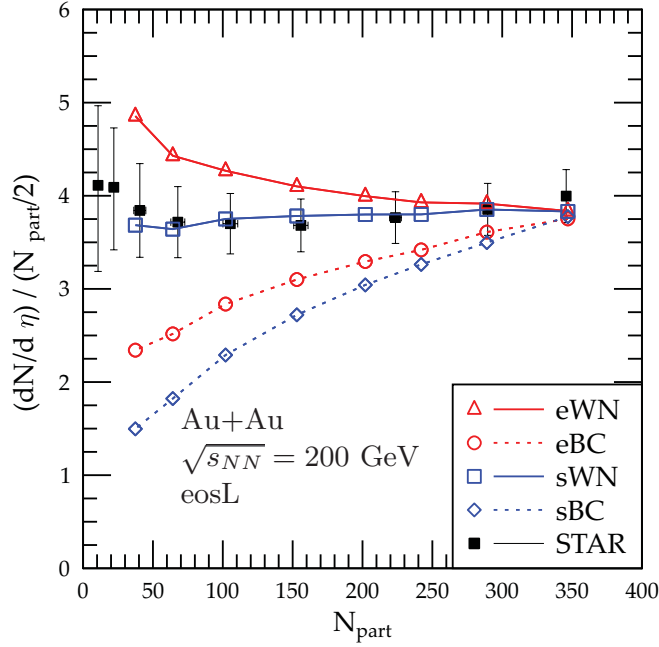
FIG. 1. (Color online) Number of charged hadrons at midrapidity in $\sqrt{s_{NN}} = 200$ GeV Au + Au collisions scaled by the number of the participant pairs calculated from the optical Glauber model. The data are from the STAR Collaboration [28].

different cases. The first case, called here "eosQ," corresponds to the bag-model EoS with a first-order phase transition [32]. In eosQ, the high-temperature phase with the bag constant is an ideal gas of three flavors of massless quarks and gluons, while the low-temperature phase is an ideal gas of all hadronic states with $m < 2$ GeV. These two phases are connected with a mixed phase, and the bag constant is chosen so that the critical temperature is $T_c = 165$ MeV. The second EoS case, which we call "eosL," is adopted from Ref. [33]. This EoS is quite similar to the recently constructed lattice EoS "s95-p" [34], and, as discussed in Ref. [34], the hadron spectra and elliptic flow are in practice insensitive to the differences between eosL and s95-p.

Since the lattice data suggest that the phase transition from the QGP to hadron gas (HG) is not of first order, one may consider the eosQ case somewhat unrealistic. However, the computation of thermal photon production in the phase-transition region requires well-defined QGP and hadron-gas fractions, which are available only in the eosQ case. With eosL, in the absence of such phase fractions, there are additional uncertainties in the thermal photon calculation related to the QGP and HG emission rates.

Thermal transverse momentum (p_T) spectra of hadrons are obtained using the Cooper-Frye method [35], where particle emission from a freeze-out hypersurface σ is calculated with

$$\frac{dN^f}{d^2 p_T dy} = \int_\sigma f(x, p) p^\mu d\sigma_\mu, \qquad (4)$$

where $f(x, p)$ is the momentum distribution function of a specific hadron type. We assume the system to decouple at a single constant temperature T_{dec}, which is fixed so that we get a good agreement with the measured p_T spectra of pions at

RHIC. With eosQ, we have $T_{\text{dec}} = 140$ MeV, and 160 MeV with eosL.

After the thermal emission of particles from the freeze-out surface is calculated, we take into account the strong and electromagnetic two- and three-body decays. This treatment is essential because most of the stable particles in our case come from the decays of heavy resonances.

The p_T spectra of hadrons can be written as a Fourier series,

$$\frac{dN}{d^2 p_T dy} = \frac{1}{\pi} \frac{dN}{dp_T^2 dy} \left(1 + \sum_{n=1}^\infty 2v_n \cos(n\phi)\right), \qquad (5)$$

where ϕ is the hadron momentum's azimuthal angle with respect to the reaction plane defined by the impact parameter. Elliptic flow, v_2, is the second coefficient in this series and it can be computed from

$$v_2(p_T) = \frac{\int d\phi \cos(2\phi) \frac{dN(b)}{dp_T^2 d\phi dy}}{\int d\phi \frac{dN(b)}{dp_T^2 d\phi dy}}. \qquad (6)$$

Correspondingly, the p_T-integrated v_2 becomes

$$v_2 = \frac{\int d\phi \cos(2\phi) \frac{dN(b)}{d\phi dy}}{\int d\phi \frac{dN(b)}{d\phi dy}}. \qquad (7)$$

D. Thermal photons emission from the hydrodynamical medium

The p_T spectra of thermal photons can be calculated from

$$\frac{dN^\gamma}{d^2 p_T dy} = \int d^4 x \, \Gamma(E^*(x), T(x)), \qquad (8)$$

where $\Gamma(E^*, T)$ is the Lorentz invariant thermal photon emission rate, $d^4 x$ is the volume element, and $E^*(x) = p^\mu u_\mu(x)$ is the photon energy in the fluid's local rest frame. For the QGP, we use the emission rate from Refs. [36,37] with $N_f = 3$ and a running strong coupling constant [38] $\alpha_s = \beta / \ln(8T/\Lambda)$, with $\beta = 6\pi/(33 - 2N_f)$ and $\Lambda = 200$ MeV. For the hadron gas, we use two different emission rates: (i) The first are those calculated in Refs. [39,40] and parametrized in Refs. [40,41], which we call "R92." Also the a_1 exchange in $\pi + \rho \rightarrow \rho + \gamma$ is taken into account as suggested in Ref. [42]. These rates were used in the previously published LHC predictions [21]. (ii) The second are the more recent ones from Ref. [43] which account also for the finite size of hadrons through form factors. We call these rates "TRG."

With eosL, which smoothly goes from the QGP to the HG phase without specifying their volume fractions, one needs to choose how to switch from the QGP to HG photon emission rates. For simplicity, we choose to do this at a constant temperature T_s but we vary T_s between 170 and 200 MeV. We label these two cases as "eosL170" and "eosL200." We emphasize that instead of an *ad hoc* modeling of volume fractions, we consider these two limiting cases to get a handle on the uncertainties related to the rate-switching procedure.

To illustrate the differences between the R92 and TRG emission rates, which are important for the photonic v_2 results presented in Sec. III, we plot in Fig. 2 the ratio of the photon emission rates in the HG and QGP at two different fixed
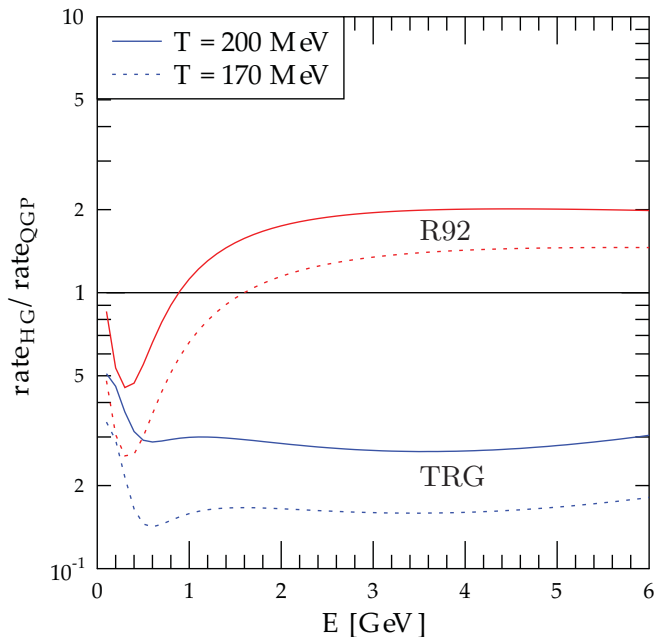
FIG. 2. (Color online) The HG-to-QGP ratio of the photon emission rates as a function of the photon energy at two different temperatures. Two different HG rates, R92 [39–41] and TRG [43], are compared.
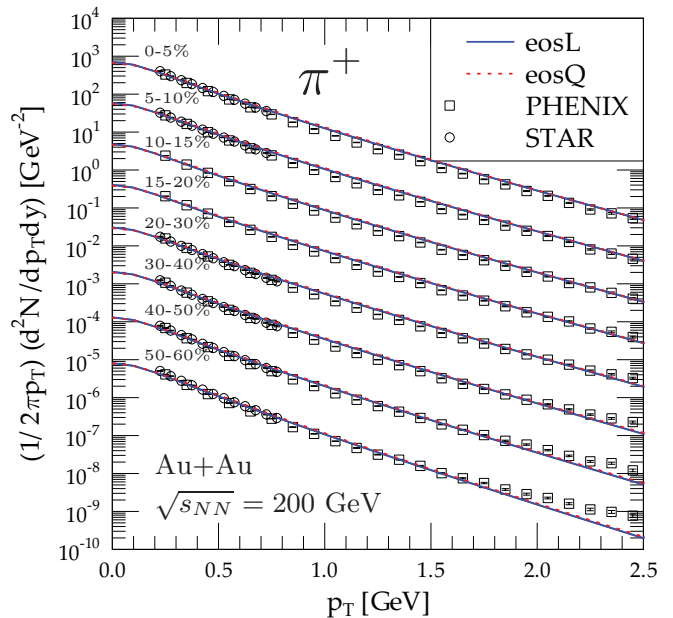

FIG. 3. (Color online) The p_T spectra of positive pions for $\sqrt{s_{NN}} = 200$ GeV Au + Au collisions at RHIC compared with the PHENIX data [44]. The centrality classes are indicated in the figure and the spectra are scaled by increasing powers of 10^{-1}.

temperatures. We see that (since both HG rates have been divided by the same QGP rate) the difference between R92 and TRG is about a factor of 6 at large energies. Furthermore, the TRG rates are always well below the QGP rates, whereas this is not the case for the R92 rates.

Elliptic flow for the thermal photons is calculated as in Eq. (6). Since the thermal photons cannot be distinguished from other direct photons, the elliptic flow from thermal photons alone cannot be measured. In what follows, we assume that the net contribution to the photonic v_2 from the other direct photon sources remains small, especially since the fragmentation photons with a positive v_2 should partially cancel the negative v_2 of the photons arising from parton-medium interactions [9].

If other components are emitted isotropically we can roughly estimate how much they "wash away" the elliptic flow coming from thermal photons. The total elliptic flow is then

$$v_2 = \left(\int d\phi \cos(2\phi) \frac{dN^{\text{th}}}{dp_T^2 d\phi dy} \right) \left(\int d\phi \frac{dN^{\text{all}}}{dp_T^2 d\phi dy} \right)^{-1} \quad (9)$$

$$= v_2^{\text{th}} \left(\frac{dN^{\text{th}}}{dp_T^2 dy} \right) \left(\frac{dN^{\text{all}}}{dp_T^2 dy} \right)^{-1}, \quad (10)$$

where $dN^{\text{all}}/dp_T^2 dy$ corresponds to the measured p_T spectrum of direct photons and v_2^{th} is the v_2 of thermal photons alone.

III. RESULTS FOR RHIC

A. Hadron spectra and elliptic flow

First we show the hadronic observables to demonstrate that our hydrodynamical description of the bulk QCD medium is

reasonable. Figure 3 shows the transverse momentum spectra of positively charged pions in different centrality classes in $\sqrt{s_{NN}} = 200$ GeV Au + Au collisions at RHIC. As we can see, we have a good fit to the pion spectra below $p_T \approx 2$ GeV for a very wide range of centralities. The integrated elliptic flow of charged hadrons from Eq. (7) is plotted in Fig. 4 together with the data obtained by the STAR Collaboration [45] using the four-particle cumulant and Lee-Yang zeros (LYZ) methods, which should best reflect the elliptic flow relative to the reaction plane defined by the impact parameter. We have a fairly good description of the data also here, although the centrality dependence of the computed v_2 is not fully reproduced. We expect, however, that fine-tuning the initial density profile, invoking the Monte Carlo Glauber model and possibly also event-by-event hydrodynamics (see, e.g., Ref. [46]) as well as including viscous effects (see, e.g., Ref. [47]), will improve the agreement. These improvements are, however, beyond the scope of this exploratory paper.

B. Photon spectra

To study how much elliptic flow is washed away by other sources of direct photons at RHIC, we need to estimate the other components. We do this by fitting the measured photon p_T spectrum. To study the uncertainties due to the chosen fit functions, we use two different forms. Our first choice (fit 1) is an exponential combined with a power-law function [20]:

$$f(p_T) = A \exp(-p_T/T) + \frac{C}{\left(1 + p_T^2/b\right)^n}, \quad (11)$$

where A, T, C, b, and n are the fit parameters. This fit function is physically motivated by the QCD-like power-law behavior
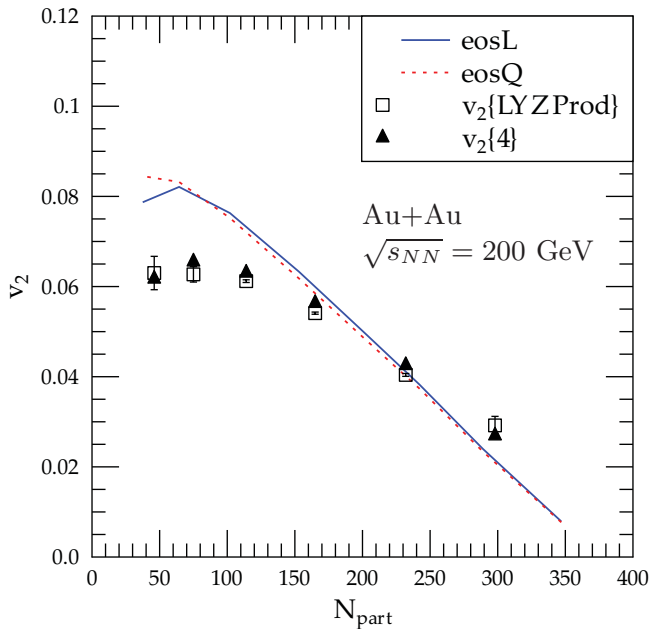
FIG. 4. (Color online) The integrated v_2 for charged hadrons in $\sqrt{s_{NN}} = 200$ GeV Au + Au collisions at RHIC compared with the STAR data [45].

at high p_T and the thermal-like exponential at low p_T. Our alternative choice (fit 2) is a mere power-law function:

$$f(p_T) = \frac{C}{\left(1 + p_T^2/b\right)^n}.\tag{12}$$

In these fits, we use the photon data from the PHENIX Collaboration. The older data sets [18,19] have large error bars at low p_T, but in the more recent low-p_T data [20] the error bars are much smaller. Unfortunately, the centrality classes in these measurements differ from each other. For our fits shown in Fig. 5, we have simply combined the 0–20% (20–40%) centrality data from Ref. [20] with the 10–20% (30–40%) centrality data from Ref. [19]. In our fits we included all data points from the aforementioned sets.

With fit 1, we first find the parameters b and n by fitting the measured photon p_T spectra in $p + p$ collisions using the PHENIX data [18,20] shown in Fig. 5(a). Then for the Au + Au case, keeping the high-p_T slope parameters b and n fixed, we find A, T, and C by fitting the PHENIX data [19,20] for the two centrality classes shown in Fig. 5. For fit 2, we use the same data sets. The best fit parameters obtained for the power-law fits are listed in Table II and the parameters for fit 1 can be found in Table III. Fits 1 and 2 have equally small χ^2 values at both centralities.

TABLE II. The parameters obtained for the power-law fits 2.

	C (GeV^{-2})	b (GeV^2)	n
$p + p$	3.29×10^{-1}	4.37×10^{-1}	3.09
Au + Au 0–20%	2.16×10^{14}	5.24×10^{-5}	3.35
Au + Au 20–40%	9.33×10^{17}	6.35×10^{-6}	3.52

TABLE III. The parameters for the exponential + power-law fits 1. In this case, n and b are obtained from Table II.

	A (GeV^{-2})	T (GeV)	C
Au + Au 0–20%	85.4	0.212	4.96
Au + Au 20–40%	30.7	0.218	1.18

In Fig. 5(b) we replot the low- and mid-p_T region from Fig. 5(a) and show our thermal photon results obtained with eosL (eosQ) using the TRG (R92) rates in the HG phase. For clarity, we plot the eosL results only for $T_s = 170$ MeV. If we do the switch of the emission rate at $T_s = 200$ MeV, we get 30% (10%) fewer photons at $p_T = 1(2)$ GeV, because the TRG emission rate is smaller than the QGP emission rate, as shown in Fig. 2.

Our thermal photon results shown in Fig. 5(b) differ by a factor of 2 at high p_T. Some of this difference comes from the small difference in the initial temperature profiles, which in our case are obtained from the fixed initial entropy density through the EoS. However, a more dominant effect is the different mapping of the energy density to the temperature in eosQ and eosL. The difference in the actual temperature in the two cases is not large but the exponential temperature dependence in the emission rates magnifies the effect considerably.

From the previous photon studies (see, e.g., Refs. [11,12]), we know that photons from HG are contributing mostly at small p_T. In Fig. 5 the difference between the eosQ+R92 and eosL+TRG results shrinks down at low p_T because the R92 HG emission rate is larger than that in the TRG rates and because with eosQ the HG volume becomes larger than with eosL. When we use the TRG rates and eosL, only 3% of the photons come from the HG at $p_T = 1$ GeV. With eosQ and the R92 rates, about 50% of the photons originate from HG at the same p_T.

We also note that in the low-p_T region our thermal photon results very clearly undershoot the latest PHENIX data. We checked that changing the freeze-out temperature to $T_{\text{dec}} = 120$ MeV gives only a negligible improvement. This feature is typical to almost all hydrodynamical calculations, as can been seen, for example, from Fig. 43 in Ref. [48].

At $p_T \sim 3$ GeV the obtained thermal photon emission is almost enough to match fit 1 at both centralities if eosL is considered. This suggests that we may have a window for thermal photon dominance at this p_T. However, if we compare with fit 2, there is always at least a factor-of-2 difference. Event-by-event fluctuations in the initial state, however, were shown to increase the thermal emission at $p_T > 2$ GeV [49], and thus we should indeed have a better chance to have a region where the direct photon p_T spectrum, and consequently also the photon v_2, at RHIC is entirely dominated by the thermal emission.

C. Photon elliptic flow

In Fig. 6(a) we plot the elliptic flow of the thermal photons using both eosQ and eosL with the R92 rates. Figure 6(b) shows the same calculations but with the TRG rates. Unlike
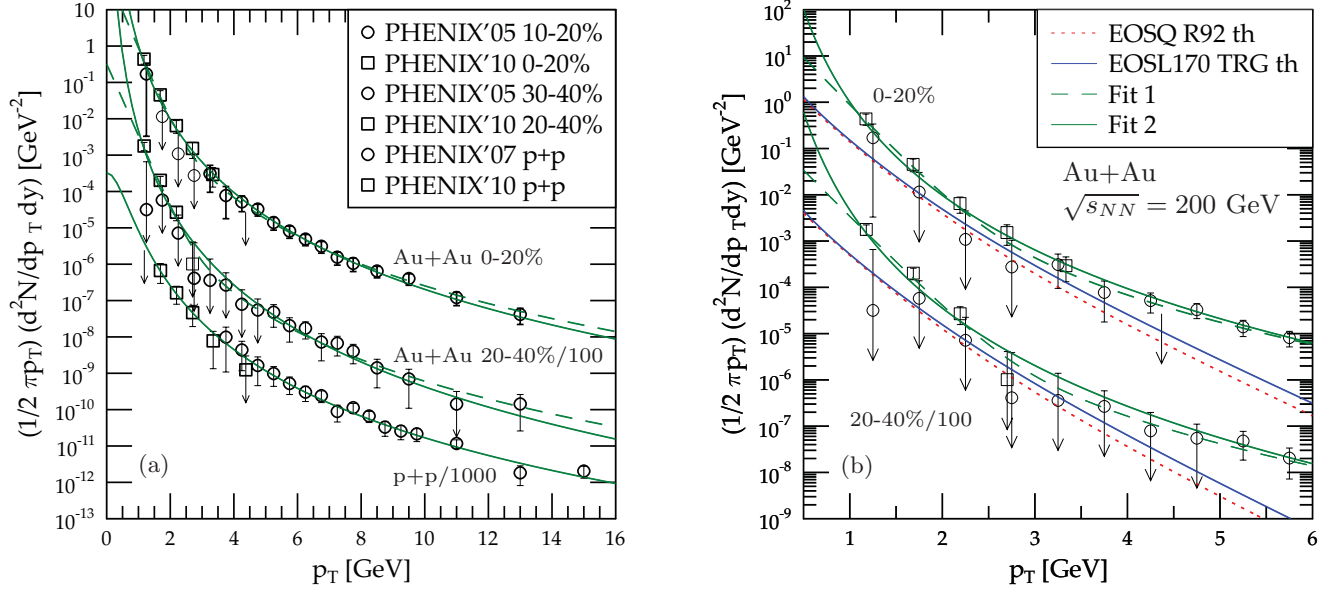
FIG. 5. (Color online) The fits 1 and 2 to the measured photon spectra for two different centralities in $\sqrt{s_{NN}} = 200$ GeV Au + Au collisions and in $p + p$ collisions at $\sqrt{s} = 200$ GeV. The 20–40% centrality-class spectra are divided by 100 and the $p + p$ case by 1000. The data are from the PHENIX Collaboration [18–20]. Our thermal photon results are shown in (b).

for hadrons, the thermal photon elliptic flow starts to decrease quickly above $p_T \sim 2$ GeV. The reason for this is that practically all high-p_T photons are emitted nearly isotropically in the beginning of the evolution (see, e.g., Fig. 3 in Ref. [49]), when the hydrodynamical flow effects are very small. Because the photon emission is dominated by the early times the thermal photon elliptic flow is clearly smaller than the hadronic $v_2(p_T)$, which probes the flow anisotropy only on the freeze-out surface.

From Fig. 6(a) we see that the larger switching temperature T_s in eosL only moves the elliptic-flow peak toward higher p_T. However, as shown in Fig. 6(b), with the TRG rates there is factor-of-2 difference in the maximum value between the eosL170 and eosL200 cases. This systematics can be deduced from Fig. 2 and hydrodynamical evolution as follows: When the system reaches the crossover region near the QCD phase transition, there has already been a significant anisotropy developed in the transverse flow which is directly reflected to the thermal photon v_2. Thus, if the photon emission is increased (decreased) in this region, the thermal photon v_2 increases (decreases). As seen in Fig. 2, with the TRG rates the QGP emission rate is larger than the HG rate. Hence, increasing the switching temperature decreases the emission and thus the v_2. This effect is seen in Fig. 6(b). With the R92 rates in Fig. 6(a) the situation is slightly different, as in the crossover region $T = 170$–200 MeV the QGP emission rate is larger than the HG rate at small energies and vice versa at high energies. Thus, at low p_T in Fig. 6(a) the situation is similar to that in Fig. 6(b) (i.e., v_2 is larger for eosL170 than for eosL200). At $p_T > 2$ GeV, the increase of the switching temperature now increases the total emission, thus making v_2 larger for eosL200 than for eosL170.

We also notice from the eosQ results in Fig. 6 that the maximum v_2 decreases by a factor of 2 when we replace the

R92 rates with the TRG rates. Because the QGP rates in both cases are the same, this signals to us that the hadron gas indeed plays an important role in generating the thermal photon v_2 in the eosQ case. To quantify this statement, we plot in Fig. 7 the fraction of photons $v_2(p_T)$ coming from the HG phase. We define v_2^{HG} as

$$v_2^{\mathrm{HG}} = \frac{\int d\phi \cos(2\phi) \frac{dN^{\mathrm{HG}}}{dp_T^2 d\phi dy}}{\int d\phi \frac{dN^{\mathrm{QGP+HG}}}{dp_T^2 d\phi dy}}, \tag{13}$$

that is, relative to all thermal photons. We see that the photon v_2 can be mostly from the HG (eosQ with R92), mostly from the QGP (eosL170 with TRG), or between these extremes (eosQ + TRG and eosL170 + R92). Thus, both the EoS and the HG emission rate have a big effect on where the thermal photon v_2 originates from.

Figure 8 illustrates how much elliptic flow of thermal photons is washed away if we include other direct photon components, assuming that they are produced isotropically. We can see that the final photon v_2, obtained from Eq. (9) based on fits 1 and 2, is clearly smaller than the thermal one and also that the different fit functions modify the place and shape of the peak, keeping the maximum v_2 roughly the same, however.

In Fig. 9, we plot both the thermal photon and the full direct photon elliptic flow in 0–20% and 20–40% centrality classes for the eosQ + R92 and eosL170 + TRG cases. The latter can be considered a state-of-the-art calculation in that a realistic EoS and the latest rates are utilized. In the eosQ+R92 case, the elliptic flow is as large as it can be in our approach. For both cases, fit 1 is used to estimate how the other components reduce the elliptic flow. As seen in Fig. 5, the thermal photon yield is smaller in the eosQ case, and hence the other direct
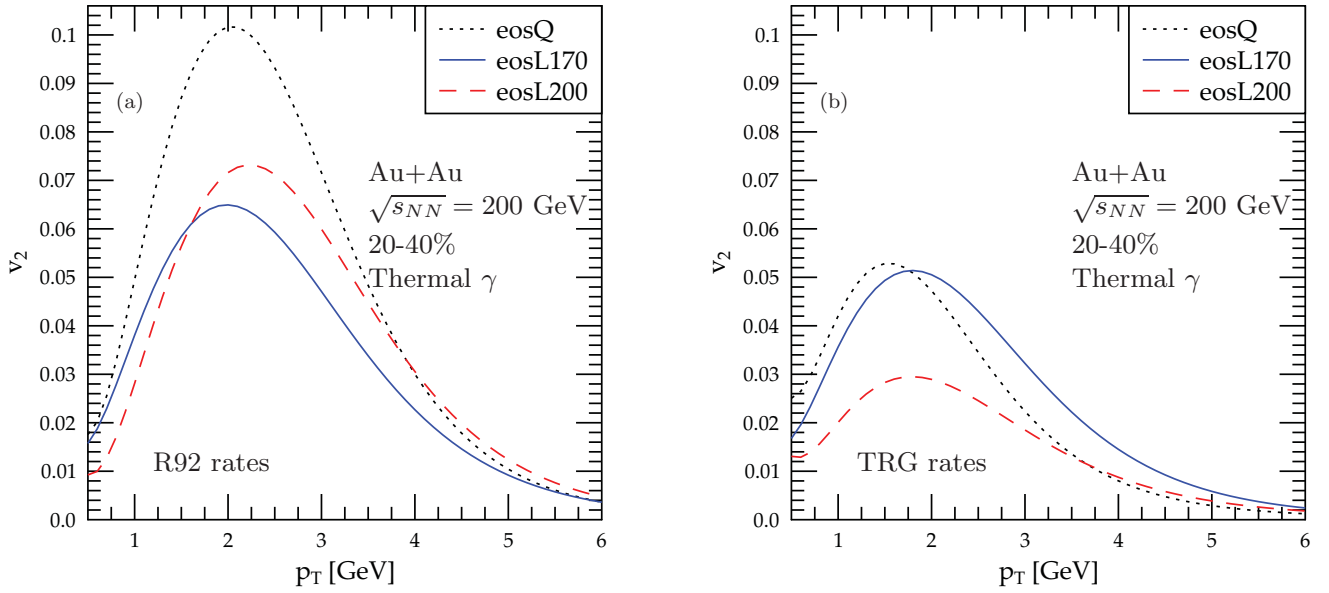
FIG. 6. (Color online) Elliptic flow of thermal photons in Au + Au collisions at $\sqrt{s_{NN}} = 200$ GeV.

photon components wash away more of the elliptic flow in the eosQ case than in eosL170 case.

Finally, in Fig. 10 we compare our calculations with photon v_2 data measured by the PHENIX Collaboration [50].[2] The PHENIX result is obtained using the event plane from hadrons whereas our calculations are made with respect to the reaction plane. This means that the calculated and measured v_2 should not necessarily coincide, but if the situation is similar to

the hadronic case, their difference should not be larger than ~20% [46]. As seen in the figure, the measured value at the peak is much larger than the thermal photon v_2. Because even our maximal v_2 case, eosQ + R92, is below the data, we study how much more v_2 could be generated by lowering the decoupling temperature down to $T_f = 120$ MeV. We emphasize, however, that with this low T_f the hydrodynamical calculation overshoots the measured pion p_T spectra [24]. We observe that even with a lower T_f the thermal photon v_2 remains too small. Also the eosL170 + TRG results with two different T_fs are shown in the figure.

_____

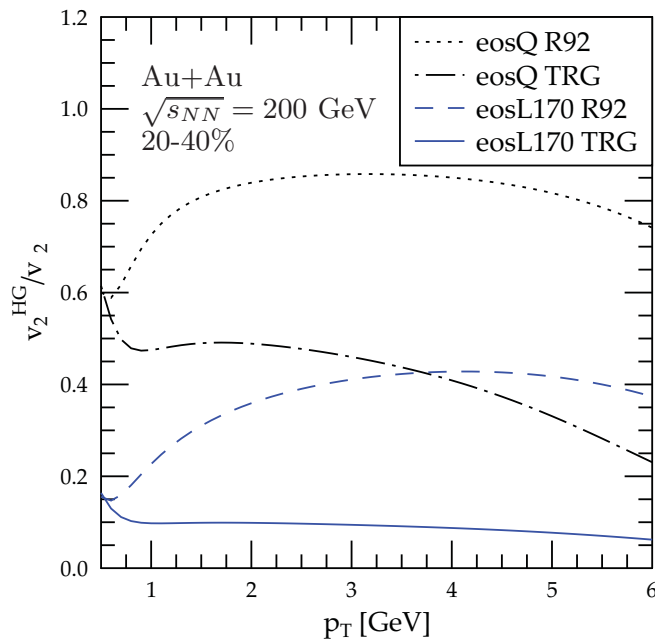[2]These data were published during the review process of this paper.

FIG. 7. (Color online) The contribution to the thermal photon elliptic flow from the hadron gas in Au + Au collisions at $\sqrt{s_{NN}} = 200$ GeV.
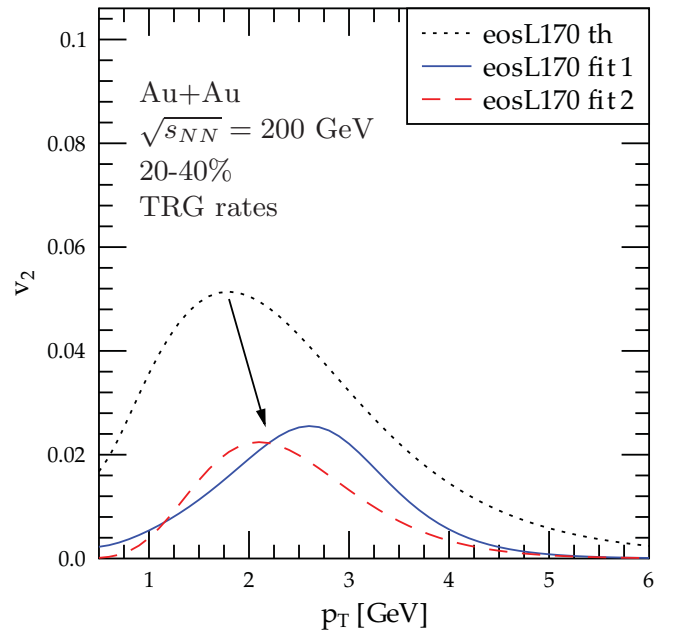

FIG. 8. (Color online) Elliptic flow of thermal and direct photons in Au + Au collisions at $\sqrt{s_{NN}} = 200$ GeV.
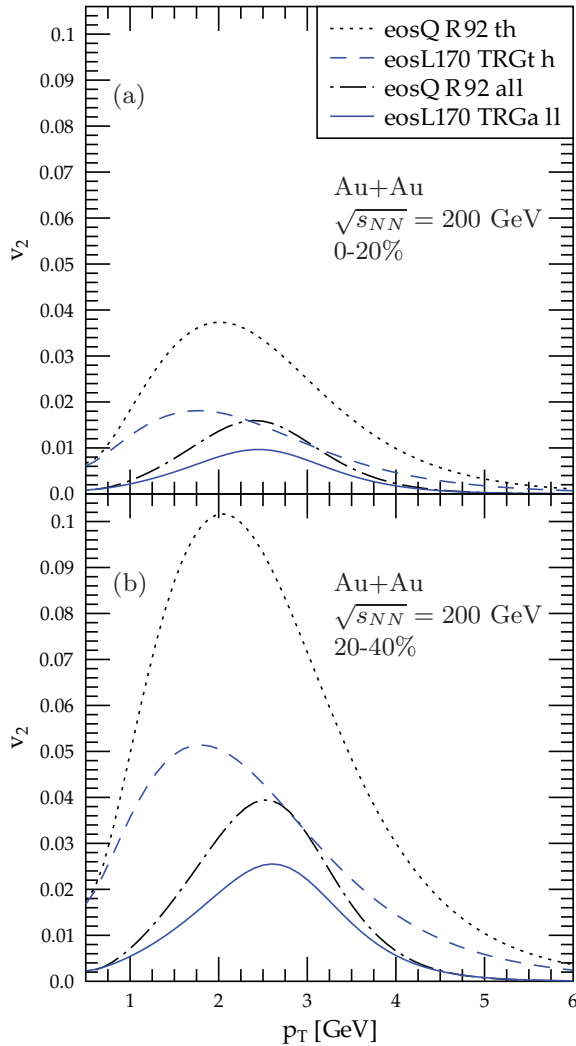
FIG. 9. (Color online) Elliptic flow of direct photons in Au + Au collisions at $\sqrt{s_{NN}} = 200$ GeV.

IV. PREDICTION FOR THE LHC

Next, we extrapolate our hydrodynamical modeling to the $\sqrt{s_{NN}} = 2.76$ TeV Pb + Pb collisions at the LHC. We choose the same sWN initial density profile and decoupling temperatures as at RHIC, and, as explained in Sec. II B, use the measured charged-hadron multiplicity [26] to fix the initial entropy and initial time through the EKRT model (for details, see Ref. [27]). As seen in Fig. 11, a reasonable agreement with the measured charged-hadron p_T spectrum [51] follows up to $p_T \sim 4$ GeV. This ensures that our thermal photon calculations are meaningful also at the LHC energies.

In Fig. 12 we plot our prediction for the thermal photon p_T spectrum in the $\sqrt{s_{NN}} = 2.76$ TeV Pb + Pb collisions at the LHC. The bands shown are defined by the cases eosL170 + R92 and eosQ + TRG, which give the largest and smallest yields, correspondingly. We see that the uncertainty coming from the EoS and from the HG emission rates is at its largest, of the order of 40%. We note that these predictions are qualitatively quite similar to the predictions given in Refs. [21,22] for $\sqrt{s_{NN}} = 5.5$ TeV.
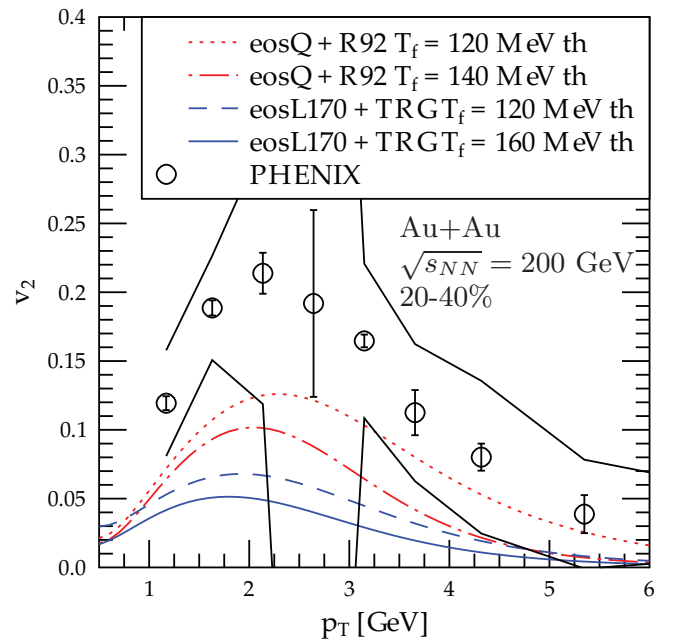

FIG. 10. (Color online) Elliptic flow of thermal photons in Au + Au collisions at $\sqrt{s_{NN}} = 200$ GeV with two different freeze-out temperatures compared with the PHENIX Collaboration measurement [50].

Since currently we do not have the measured total direct photon spectrum at the LHC available yet (as we had at RHIC), we can consider only the thermal photon elliptic flow here. It is, however, very interesting to compare the thermal photon elliptic flow with the RHIC results. We plot the obtained thermal photon v_2 in Fig. 13 for 20–40% central collisions. We can see that, similarly to the hadronic case [52], the
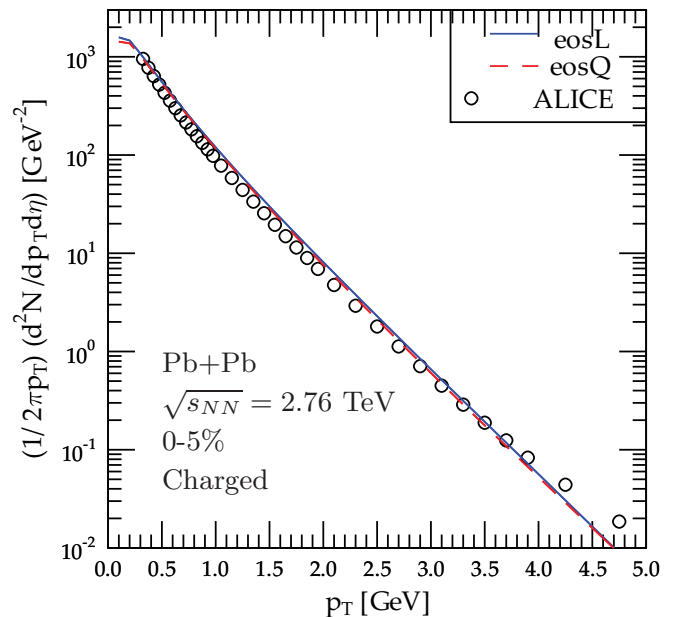

FIG. 11. (Color online) Transverse momentum spectra of charged hadrons in 0–5% most central Pb + Pb collisions at $\sqrt{s_{NN}} = 2.76$ TeV. Data from the ALICE Collaboration [51].
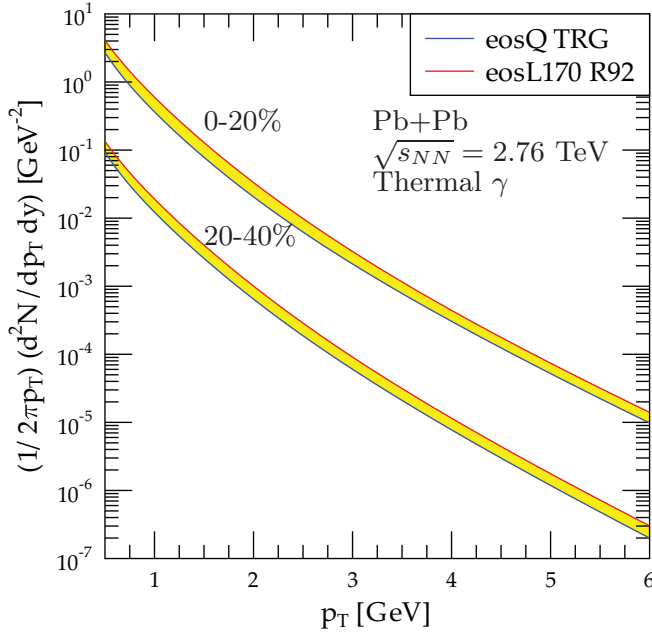
FIG. 12. (Color online) Transverse momentum spectra of thermal photons in Pb + Pb collisions at $\sqrt{s_{NN}} = 2.76$ TeV.

FIG. 13. (Color online) Elliptic flow of thermal photons in Pb + Pb collisions at $\sqrt{s_{NN}} = 2.76$ TeV.

thermal photon elliptic flow is very similar at RHIC and LHC. This is a nontrivial result because the temperature range, flow range, as well as the volume factors for photon emission (from the QGP in particular) are larger at the LHC than at RHIC, and, as discussed in Ref. [25], also the flow asymmetry near the phase transition region is larger at the LHC. Then, when going from RHIC to LHC, to arrive at a similar v_2 in both cases, the increased flow asymmetry in the numerator of Eq. (6) is compensated by the increased photon yields in the denominator of Eq. (6). In Fig. 14 we again plot the hadronic fraction of $v_2(p_T)$ for the same cases as in Fig. 7. The figure shows that v_2^{HG} is again very close to the corresponding fraction at RHIC.

V. DISCUSSION

We considered the sensitivity of thermal photon production to the EoS and emission rates in heavy-ion collisions at RHIC and LHC. We compared the obtained thermal photon yields with the PHENIX measurements and showed that in the window $2 \lesssim p_T \lesssim 3$ GeV the thermal contribution, computed with a realistic EoS (eosL) and the latest emission rates (TRG), is reasonably close to the data. As in most previous hydrodynamical studies, in the region $p_T \sim 1$ GeV, however, we get a clearly smaller yield than what was measured most recently. We show that around $p_T \sim 2$ GeV the thermal photon elliptic flow peaks at a fairly large value, 5% in the 20–40% centrality class with eosL + TRG, but also that the possible other components may wash even half of this away. We emphasize, however, that the amount of v_2 washout depends on the thermal photon contribution relative to the other components. Thermal photon production near $p_T \sim 2$ GeV at RHIC can be expected to increase further once the
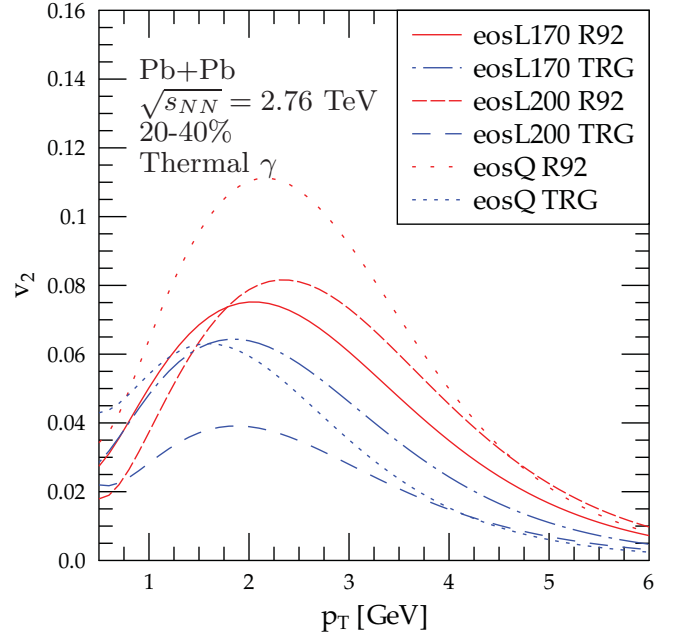
event-by-event QCD-matter density fluctuations are accounted for [49], in which case the thermal photon production can become dominant and the v_2 washout can decrease or even vanish.

The direct photon elliptic flow measured by the PHENIX Collaboration [50] is much higher than any of our results. Excitingly, this suggests the dominance of thermal photons
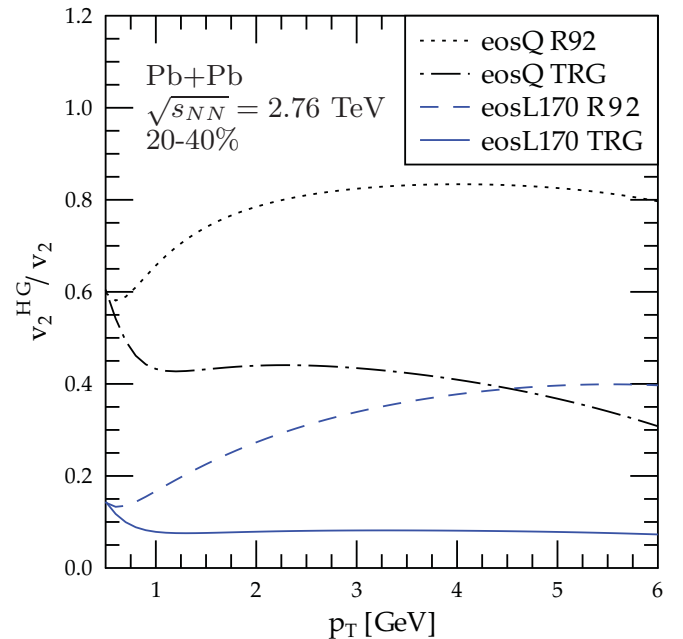

FIG. 14. (Color online) The contribution to the thermal photon elliptic flow from the hadron gas in Pb + Pb collisions at $\sqrt{s_{NN}} = 2.76$ TeV.

near $p_T \sim 2$ GeV. However, the origin of such large v_2 cannot be explained in the current framework.

Constraining our hydrodynamical modeling with the measured charged-hadron spectrum in $\sqrt{s_{NN}} = 2.76$ TeV Pb + Pb collisions at the LHC, we predicted the thermal photon p_T spectra and v_2. According to our results, elliptic flow of thermal photons at the LHC and RHIC are very similar in the few-p_T region. However, one should keep in mind that we cannot fully explain the direct photon v_2 at RHIC. For the determination of a possible thermal photon window, and consequently thermal photon v_2, it will be extremely interesting to see the direct photon data at the LHC.

Next, one should consider the effects of event-by-event density fluctuations [46,53–57] on thermal photon elliptic flow. On the theoretical side, one would need a better understanding of how the degrees of freedom in the QGP would be best accounted for when computing thermal photon production, as well as a better control over the photon emission in the phase-transition region. Also the dissipative hydrodynamical effects to thermal photon production should be studied further; so far only the very first steps have been taken in this direction (see Ref. [58]).

[1] PHENIX Collaboration, S. S. Adler *et al.*, Phys. Rev. Lett. **96**, 202301 (2006).

[2] P. Aurenche, J.-P. Guillet, E. Pilon, M. Werlen, and M. Fontannaz, Phys. Rev. D **73**, 094007 (2006).

[3] F. Arleo, K. J. Eskola, H. Paukkunen, and C. A. Salgado, J. High Energy Phys. 04 (2011) 055.

[4] K. J. Eskola, H. Paukkunen, and C. A. Salgado, J. High Energy Phys. 04 (2009) 065.

[5] R. J. Fries, B. Muller, and D. K. Srivastava, Phys. Rev. Lett. **90**, 132301 (2003).

[6] R. J. Fries, B. Muller, and D. K. Srivastava, Phys. Rev. C **72**, 041902 (2005).

[7] S. Turbide, C. Gale, E. Frodermann, and U. Heinz, Phys. Rev. C **77**, 024909 (2008).

[8] F.-M. Liu, T. Hirano, K. Werner, and Y. Zhu, Phys. Rev. C **79**, 014905 (2009).

[9] G.-Y. Qin, J. Ruppert, C. Gale, S. Jeon, and G. D. Moore, Phys. Rev. C **80**, 054909 (2009).

[10] P. Huovinen, P. V. Ruuskanen, and J. Sollfrank, Nucl. Phys. A **650**, 227 (1999).

[11] P. Huovinen, P. V. Ruuskanen, and S. S. Räsänen, Phys. Lett. B **535**, 109 (2002).

[12] S. S. Räsänen, Nucl. Phys. A **715**, 717 (2003).

[13] D. G. d'Enterria and D. Peressounko, Eur. Phys. J. C **46**, 451 (2006).

[14] R. Chatterjee, E. S. Frodermann, U. W. Heinz, and D. K. Srivastava, Phys. Rev. Lett. **96**, 202302 (2006).

[15] R. Chatterjee and D. K. Srivastava, Phys. Rev. C **79**, 021901 (2009).

[16] F.-M. Liu, T. Hirano, K. Werner, and Y. Zhu, Phys. Rev. C **80**, 034905 (2009).

[17] N. Armesto *et al.*, J. Phys. G **35**, 054001 (2008).

[18] PHENIX Collaboration, S. S. Adler *et al.*, Phys. Rev. Lett. **98**, 012002 (2007).

[19] PHENIX Collaboration, S. S. Adler *et al.*, Phys. Rev. Lett. **94**, 232301 (2005).

[20] PHENIX Collaboration, A. Adare *et al.*, Phys. Rev. Lett. **104**, 132301 (2010).

[21] F. Arleo *et al.*, arXiv:hep-ph/0311131.

[22] K. Dusling and I. Zahed, Phys. Rev. C **82**, 054909 (2010).

[23] K. J. Eskola, K. Kajantie, P. V. Ruuskanen, and K. Tuominen, Nucl. Phys. B **570**, 379 (2000).

[24] K. J. Eskola, H. Honkanen, H. Niemi, P. V. Ruuskanen, and S. S. Rasanen, Phys. Rev. C **72**, 044904 (2005).

[25] H. Niemi, K. J. Eskola, and P. V. Ruuskanen, Phys. Rev. C **79**, 024903 (2009).

[26] ALICE Collaboration, K. Aamodt *et al.*, Phys. Rev. Lett. **105**, 252301 (2010).

[27] T. Renk, H. Holopainen, R. Paatelainen, and K. J. Eskola, Phys. Rev. C **84**, 014906 (2011).

[28] STAR Collaboration, B. I. Abelev *et al.*, Phys. Rev. C **79**, 034909 (2009).

[29] P. F. Kolb, U. W. Heinz, P. Huovinen, K. J. Eskola, and K. Tuominen, Nucl. Phys. A **696**, 197 (2001).

[30] J. P. Boris and D. L. Book, J. Comput. Phys. **A11**, 38 (1973).

[31] S. T. Zalesak, J. Comput. Phys. A **31**, 335 (1979).

[32] J. Sollfrank, P. Huovinen, M. Kataja, P. V. Ruuskanen, M. Prakash, and R. Venugopalan, Phys. Rev. C **55**, 392 (1997).

[33] M. Laine and Y. Schroder, Phys. Rev. D **73**, 085009 (2006).

[34] P. Huovinen and P. Petreczky, Nucl. Phys. A **837**, 26 (2010).

[35] F. Cooper and G. Frye, Phys. Rev. D **10**, 186 (1974).

[36] P. B. Arnold, G. D. Moore, and L. G. Yaffe, J. High Energy Phys. 11 (2001) 057.

[37] P. B. Arnold, G. D. Moore, and L. G. Yaffe, J. High Energy Phys. 12 (2001) 009.

[38] F. Karsch, Z. Phys. C **38**, 147 (1988).

[39] J. I. Kapusta, P. Lichard, and D. Seibert, Phys. Rev. D **44**, 2774 (1991).

[40] L. Xiong, E. V. Shuryak, and G. E. Brown, Phys. Rev. D **46**, 3798 (1992).

[41] H. Nadeau, J. I. Kapusta, and P. Lichard, Phys. Rev. C **45**, 3034 (1992).

[42] C. Song, Phys. Rev. C **47**, 2861 (1993).

[43] S. Turbide, R. Rapp, and C. Gale, Phys. Rev. C **69**, 014903 (2004).

[44] PHENIX Collaboration, S. S. Adler *et al.*, Phys. Rev. C **69**, 034909 (2004).

[45] STAR Collaboration, B. I. Abelev *et al.*, Phys. Rev. C **77**, 054901 (2008).

[46] H. Holopainen, H. Niemi, and K. J. Eskola, Phys. Rev. C **83**, 034901 (2011).

[47] P. Romatschke and U. Romatschke, Phys. Rev. Lett. **99**, 172301 (2007).

[48] PHENIX Collaboration, A. Adare *et al.*, Phys. Rev. C **81**, 034911 (2010).

[49] R. Chatterjee, H. Holopainen, T. Renk, and K. J. Eskola, Phys. Rev. C **83**, 054908 (2011).

[50] PHENIX Collaboration, A. Adare *et al.*, arXiv:1105.4126, Phys. Rev. Lett. (to be published).

[51] ALICE Collaboration, K. Aamodt *et al.*, Phys. Lett. B **696**, 30 (2011).

[52] ALICE Collaboration, K. Aamodt *et al.*, Phys. Rev. Lett. **105**, 252302 (2010).

[53] R. P. G. Andrade, F. Grassi, Y. Hama, T. Kodama, and W. L. Qian, Phys. Rev. Lett. **101**, 112301 (2008).

[54] H. Petersen and M. Bleicher, Phys. Rev. C **81**, 044906 (2010).

[55] K. Werner, I. Karpenko, T. Pierog, M. Bleicher, and K. Mikhailov, Phys. Rev. C **82**, 044904 (2010).

[56] B. Schenke, S. Jeon, and C. Gale, Phys. Rev. Lett. **106**, 042301 (2011).

[57] Z. Qiu and U. W. Heinz, Phys. Rev. C **84**, 024911 (2011).

[58] K. Dusling, Nucl. Phys. A **839**, 70 (2010).